Climate-Carbon Interactions in the Current Century

# Assessment of carbon cycle potential predictability

## *Deliverable 2.1*

Authors: Bernardello R., Bopp L., Ilyina T., Mignot J., Ruprich-Robert Y. and Spring A.

This project received funding from the Horizon 2020 programme under the grant agreement No. 821003.

# Document Information

| | |
|---|---|
| GRANT AGREEMENT | 821003 |
| PROJECT TITLE | Climate Carbon Interactions in the Current Century |
| PROJECT ACRONYM | 4C |
| PROJECT START DATE | 1/6/2019 |
| RELATED WORK PACKAGE | WP2 |
| RELATED TASK(S) | T2.1 |
| LEAD ORGANIZATION | BSC |
| AUTHORS | **Bernardello R., Bopp L., Ilyina T., Mignot J., Ruprich-Robert Y. and Spring A.** |
| SUBMISSION DATE | x |
| DISSEMINATION LEVEL | PU |

# History

| DATE | SUBMITTED BY | REVIEWED BY | VISION (NOTES) |
|---|---|---|---|
| 28-5-2021 | R. Bernardello | | |
| 31-05-2021 | | P. Friedlingstein | |
| | | | |

**Please cite this report as:** Bernardello, R., Bopp, L., Ilyina, T., Mignot, J., Ruprich-Robert, Y. and Spring, A. (2021), Assessment of carbon cycle potential predictability, D2.1 of the 4C project.

**Disclaimer:** The content of this deliverable reflects only the author's view. The European Commission is not responsible for any use that may be made of the information it contains.

# Table of Contents

1 Introduction to the perfect model framework ........ 8

2 Experiment design ........ 8

2.1 IPSL-CM6A-LR ........ 8

2.2 MPI-ESM1.2-LR ........ 9

2.3 EC-Earth3-CC ........ 9

3 Potential predictability of carbon sinks ........ 10

3.1 IPSL-CM6A-LR ........ 10

3.2 MPI-ESM1.2-LR ........ 11

3.3 EC-Earth3-CC ........ 13

4 Potential predictability of ecosystem drivers ........ 15

5 Potential predictability: processes, drivers and key regions ........ 16

6 Conclusions ........ 21

7 Publications ........ 22

8 References ........ 22

# List of tables

**Table 2.1:** Characteristics of the perfect model predictions performed by each modelling group........7

# List of figures

**Figure 2.1:** Selection of starting dates for EC-Earth3-CC perfect model experiments based on their climate state as characterized by two indexes of large scale climate oscillations: the Atlantic Multi-decadal Oscillation (AMO) and the Pacific Decadal Oscillation (PDO). Starting dates were selected to represent all possible combinations. The central ellipse represents the ±1 standard deviation area....................................................8

**Figure 2.2:** Starting dates selected for EC-Earth3-CC perfect model experiment and their distribution along the temporal variability of the Southern Annular Mode.........................................................................................9

**Figure 3.1:** Comparison of the frequency content of SST (left) and CO2 fluxes (right) for various oceanic basins……………………………………………………………………………………………………………..10

**Figure 3.2:** Comparison of the mean potential prediction skill of the initialized ensemble (red) versus random uninitialized ensembles (blue) in global annual surface quantities of the carbon cycle with the anomaly correlation coefficient (ACC) on the y axis and root-mean-square-error (RMSE) on the x axis for lead years represented as dots: (a) air-sea CO2 flux, (b) air-land CO2 flux, (c) prognostic surface atmospheric CO2 , (d) diagnosed atmospheric CO2 based on oceanic carbon sink, (e) diagnosed atmospheric CO2 based on the global terrestrial carbon sink, and (f) diagnosed atmospheric CO2 based on the global oceanic and terrestrial carbon sink (see section 2.4). Error bars show 95% confidence intervals based on bootstrapping with replacement (N = 5,000). The last lead year with a bootstrapped p value (which represents that uninitialized ensembles beat initialized ensembles) lower than 5% marks the predictability horizon. Black stars with white integer denote significant lead years in ACC and RMSE, gray stars if only one metric is significant, and lead years nonsignificant in both metrics are blurred…………………………………………………………………...10

**Figure 3.3:** Probabilities of trend reduction in diagnostic atmospheric CO2 between periods of varying trend length before and after CO2 emission reductions start in 2020. PRCP2.6 (green) shows the probability of trend reduction in CO2 emission reductions scenario RCP2.6. PRCP4.5 (red) shows the probability of trend reduction in the currently most likely scenario for the near-term RCP4.5. P S (pale blue) show the probability that a change from RCP4.5 to RCP2.6 causes the respective trend reduction in a sufficient causation sense. PN (blue)show the probability that a change from RCP4.5 to RCP2.6 causes the respective trend reduction in a necessary causation sense. PNS (dark blue) shows the probability that change from RCP4.5 to RCP2.6 causes the respective trend reduction in a sufficient and necessary causation sense. Error bars show the 1% and 99% confidence intervals based on bootstrapping with replacement. Dotted lines show 99% confidence interval for time of virtual certainty in trend reduction or causation (D{S,N}). Results for policy-relevant five-year trends are highlighted in the gray box………………………………………………………………………...11

**Figure 3.4:** mean potential predictability of 2-meter air temperature (1st column), ocean surface CO2 fluxes (2nd column) and land surface CO2 fluxes (3rd column) estimated by the Anomaly Correlation Coefficient (ACC) from a perfect model approach with the EC-Earth3-CC piControl simulation. (1st row) ACC computed for the global averaged variables. The black line is the ACC computed considering the piControl trajectory as the target to predict. Each gray lines represent the ACC computed by considering a random prediction member as the target to predict (this informs on the uncertainty of our ACC estimate given the level of noise in the target to predict). The gray shading indicates the area in which the ACC is not significantly different from 0 (i.e. no more prediction skill) assessed with bootstrap resampling of the piControl simulation. The green lines indicate the ACC behavior of an hypothetical AR1 process fitted on the piControl behavior. (2nd row) ACC map computed for the forecast year 2. The stippling indicates where the ACC are not different from 0 according to bootstrap resampling. (3rd row) same as (2nd row) but for forecast year 6………………………………………...13

**Figure 4.1:** Predictability time horizon for (a) SST, (b) surface pH, (c) surface O2 and (d) NPP integrated over the top 100 m using PPP as a predictability measure. The red contour lines in panel (d) indicate the annual mean total nitrogen production in moles of nitrogen per kilogram per year averaged over the 300-year preindustrial control simulation to highlight regions with low and high NPP. In panel (d) regions north of 69◦ N and south of 69◦ S have been excluded since NPP is zero during wintertime there……………………………..14

**Figure 5.1:** standard deviation of surface CO2 fluxes computed from annual mean of the piControl simulations of (top) EC-Earth3-CC, (middle) IPSL-CM6A-LR and (bottom) MPI-ESM1-2-LR over (left) land and

(right) ocean. Note that the scales are different between land and ocean fluxes……………………………………….…...15

**Figure 5.2:** Standard deviation of annual mean surface CO2 fluxes integrated over different regions from the piControl simulations of EC-Earth3-CC (blue), IPSL-CM6A-LR (orange) and MPI-ESM1-2-LR (yellow). The box plots indicate the distribution of 21 CMIP6 piControl simulations (including the 3 models listed above). For each region the correlation (R) with the globally integrated CO2 fluxes is indicated at the bottom of the bar plot……………………………………………………………………………………………………………...16

**Figure 5.3:** Spatial correlation of the 2-meter air temperature with the time series of the land surface CO2 fluxes integrated over (top) Oceania, (2nd row) Tropical America, (3rd row) Africa and (bottom) extra-tropical Northern Hemisphere land for (left) EC-Earth3-CC, (middle) IPSL-CM6A-LR and (right) MPI-ESM1-2-LR…..17

**Figure 5.4:** same as Figure 5.3 but for the ocean surface CO2 fluxes integrated over (top) the tropical Pacific and (bottom) the Southern Ocean South of 45ºS……………………………………………………………….18

**Figure 5.5:** Predictability horizon of air-sea and air-Land co2 flux defined as latest lead year where initialised skill is better than uninitialised skill for four ESMs…………………………………………………………………18

**Figure 5.6:** Predictive skill measured by root-mean-square-error (RMSE) between the initialized ensemble mean and the target as a function of lead year for different initialization setups: perfect indicating no reconstruction and hence perfect initial conditions to predict the target (gray), indirect (green) and direct (orange). Columns show global variables: for the ocean carbon cycle (a) oceanic surface pCO2 , (b) air-sea CO2 flux; for the land carbon cycle (c) total land carbon pools, (d) air-land CO2 flux and in the atmosphere (e) atmospheric CO2 mixing ratio. (f-j) show RMSE-based predictive skill as (a-e) after mean bias reduction. Initialized ensembles are resampled with replacement (N=500) along the initialization dimension to account for initialization sampling uncertainty (see Spring and Ilyina, 2020), where errorbars show the resampled initialization skill uncertainty (±1σ). Uninitialized ensembles, shown at lead 0, are resampled from the target control simulation and show the reference skill without initialization……………………………………………….19

**Figure 5.7:** global mean temperature (top, °C) and total CO2 flux into the ocean (bottom, PgC) in the 10-mb ensemble of historical (blue) and Pacific Pacemaker (red) experiments performed with IPSL-CM6A-LR. The continuous line shows the ensemble mean and the shading the minimum and maximum values reached for each year in the 10-mb ensemble. The black line shows the data-based estimate, resulting from the average of the MPI-SOMFFN (Landschutzer et al. 2016), Jena-MLS (Roedenbeck et al. 2015) and CMEMS (Denvil-Sommer et al. 2019) products. The black-dash line shows the ocean forced simulation with NEMO-PISCES used for the Global Carbon Budget 2019 (Friedlingstein et al. 2019)..............................................................20

# About 4C

**Climate-Carbon Interactions in the Coming Century** (4C) is an EU-funded H2020 project that addresses the crucial knowledge gap in the climate sensitivity to carbon dioxide emissions, by reducing the uncertainty in our quantitative understanding of carbon-climate interactions and feedbacks. This will be achieved through innovative integration of models and observations, providing new constraints on modelled carbon-climate interactions and climate projections, and supporting Intergovernmental Panel on Climate Change (IPCC) assessments and policy objectives.

# Executive Summary

Potential predictability of global CO2 fluxes was quantified for 3 Earth System Models using perfect model predictions that took as a reference a preindustrial control simulation. Such approach assumes that the predictability of a given variable is not affected by model biases allowing to estimate for how long the memory of an initial state drives the evolution of a given variable in a given region. For global ocean CO2 fluxes, the three models show longer potential predictability ( 7-12 years) than for global land CO2 fluxes (2-5 years). Because in all models the variability of land CO2 fluxes is one order of magnitude larger than that of the ocean, the predictability horizon of atmospheric CO2 is limited by the predictability of land CO2 fluxes. An inter-model comparison of land and ocean CO2 fluxes variability revealed important differences across models on land fluxes while over the ocean models seem to broadly agree, with the high latitudes showing the largest standard deviations. However, maps of correlations between surface temperature and averaged regional CO2 fluxes revealed how the tropical Pacific variability is driving most of the land CO2 fluxes variability in all models. On the other hand, the three models show significant disagreement about the degree of control this region has over regional ocean CO2 fluxes. Preliminary analysis of the DCPP-C1.10 so-called “Pacific pacemaker experiment” pointed to a weak control of the tropical Pacific over the global ocean CO2 flux for one ESM. Another study carried out using the perfect model framework quantified the potential predictability of four marine ecosystem drivers showing how these are potentially predictable up to 3 years in advance at the surface on global scales. Finally, another study found only a marginal improvement in the potential predictability of atmospheric CO2 when direct initialization of carbon cycle variables is used, confirming that  the assimilation of physical climate variables is sufficient to reconstruct CO2 flux variations.

## Keywords

Carbon cycle, potential predictability, perfect model framework, climate variability

# 1 Introduction to the perfect model framework

In the perfect model approach we assume that the model reproduces all the processes driving the predictability of a given variable and that such representation is not affected by model biases (Boer, 2011). This approach allows to quantify the potential predictability which is an estimate of how long the memory of an initial state drives the evolution of a given variable in a given region. Such approach is well suited to establish a theoretical framework of predictability assessment across different models, as well as to investigate and better understand the processes driving predictability of the global carbon cycle. In this document we report the main results derived from Task 2.1. In Sections 2 we describe the experimental design of each modelling group, in Section 3 we provide an overall assessment of the potential predictability for each modelling system.

In Section 4 we describe the main results from a study that quantified the potential predictability of marine ecosystem drivers. Finally, in Section 5 we report on the multi-model analysis carried out to identify the key regions that drive the global CO2 fluxes variability, as well as on the analysis aimed at unveiling key process responsible for the predictability of the CO2 fluxes.

# 2 Experiment design

The three modelling groups performed a set of perfect model predictions. The main characteristics of each set together with the link to the dataset are detailed in Table 2.1.

**Table 2.1:** Characteristics of the perfect model predictions performed by each modelling group.

| Model | E/C driven | Ensemble size | N. starting dates | Length (months) | Availability |
|---|---|---|---|---|---|
| EC-Earth3-CC | C | 15 | 20 | 84 | here |
| MPI-ESM-LR | E | 9 | 12 | 120 | here |
| IPSL-CM6A-LR | C | 10 | 9 | 230 | Here here here |

## 2.1 IPSL-CM6A-LR

ENS selected 9 starting dates from the long pre-industrial control simulation performed for CMIP6. These 9 starting dates were chosen so as to sample the IPSL-CM6A-LR phases of internal variability. For each start date, 10 ensemble members are integrated over 20 years. Ensemble members are obtained by adding spatial white noise (of maximum amplitude 0.1K) to the atmospheric temperatures in the first time-step of the starting year.

## 2.2 MPI-ESM1.2-LR

MPG selected 12 starting dates from the spin up to the CMIP6 pre-industrial control simulation with prognostic atmospheric CO2, see Spring and Ilyina (2020). 9 ensemble members were created by small perturbations to an upper atmospheric mixing parameter and integrated over 20 lead years.

## 2.3 EC-Earth3-CC

To investigate whether the potential predictability of carbon sinks depends on the initial climate state of the prediction, BSC have selected 20 starting dates by sampling the main modes of decadal climate variability so to represent an ample spectrum of initial conditions.

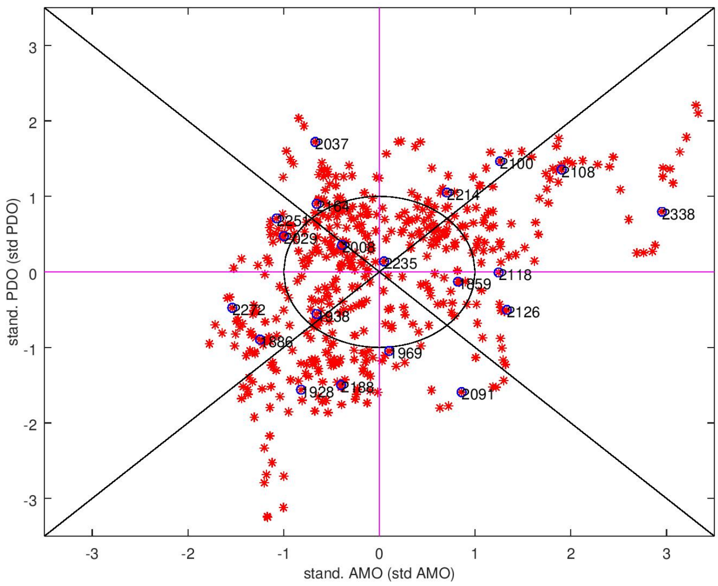


**Figure 2.1:** Selection of starting dates for EC-Earth3-CC perfect model experiments based on their climate state as characterized by two indexes of large scale climate oscillations: the Atlantic Multi-decadal Oscillation (AMO) and the Pacific Decadal Oscillation (PDO). Starting dates were selected to represent all possible combinations. The central ellipse represents the ±1 standard deviation area.

The selection of starting dates was done considering first two large scale climate indexes: the Atlantic Multi-decadal Oscillation (AMO) and the Pacific Decadal Oscillation (PDO), see Figure 2.1. Years were selected to represent as much as possible all different combinations positive/negative and moderate/strong. Moreover, the selection was done also considering other indexes known to strongly regulate CO2 fluxes to make sure to sample equally positive/negative anomalies. An example is given in Figure 2.2 for the Southern Annular Mode. From each starting, we performed 7-year predictions for 15 ensemble members that were generated by perturbing randomly initial atmospheric temperature.

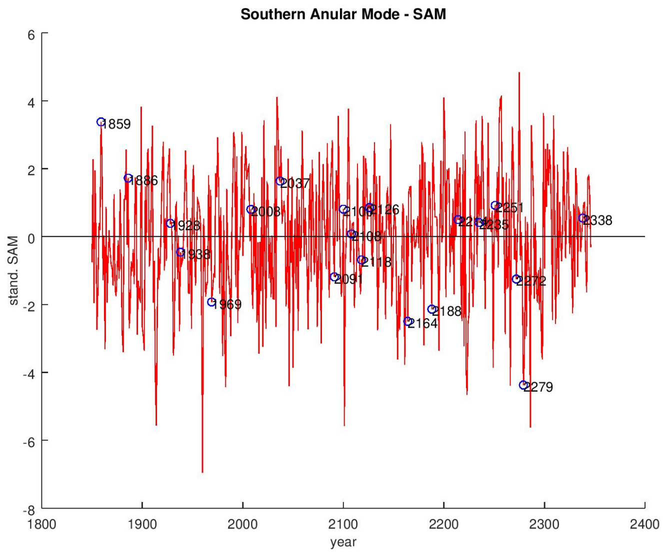


**Figure 2.2:** Starting dates selected for EC-Earth3-CC perfect model experiment and their distribution along the temporal variability of the Southern Annular Mode.

# 3 Potential predictability of carbon sinks

## 3.1 IPSL-CM6A-LR

Analysis has focused on potential predictability of air-sea CO2 fluxes. Results reveal significant prediction horizon of more than 20 years in some regions, in particular in the North Atlantic. Another region of potential predictability at the decadal timescale was found in the Southern Ocean. Both these regions are characterized in IPSL-CM6A-LR by a strong centennial variability; which explains the predictability. The North Atlantic variability is in particular driven by exchanges of salt flux with the Arctic with a ~200 yrs periodicity. Maximum frequency in the Southern Ocean is shorter (~100 yrs) and remains to be explained. This variability nevertheless does not always imprint CO2 fluxes (Figure 3.1), in particular because of a potential influence of sea ice cover as well as competing effects on different timescales. The origin of CO2 fluxes' decadal variability was further analyzed with an offline reconstruction of the CO2 fluxes. This analysis clearly shows that the relative influence of physical properties of the ocean and of biogeochemical processes strongly depends on the timescales considered. Results still require finalization, a publication will soon be prepared.

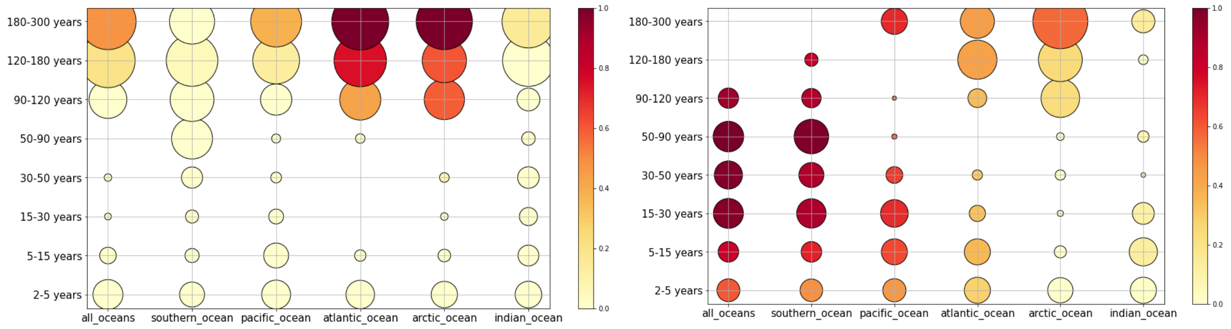


**Figure 3.1:** Comparison of the frequency content of SST (left) and CO2 fluxes (right) for various oceanic basins.

## 3.2 MPI-ESM1.2-LR

Analysis of simulations from MPG revealed robust potential predictability of global atmospheric CO2 up to 3 years, the global ocean and land CO2 fluxes are predictable for 2 years. The isolated effects of the land and ocean carbon sink on atmospheric CO2 are predictable for 5 and 12 years, respectively. Therefore, the land carbon cycle limits atmospheric CO2 predictability (Figure 3.2). This work has been published on Geophysical Research Letters (Spring and Ilyina, 2020).

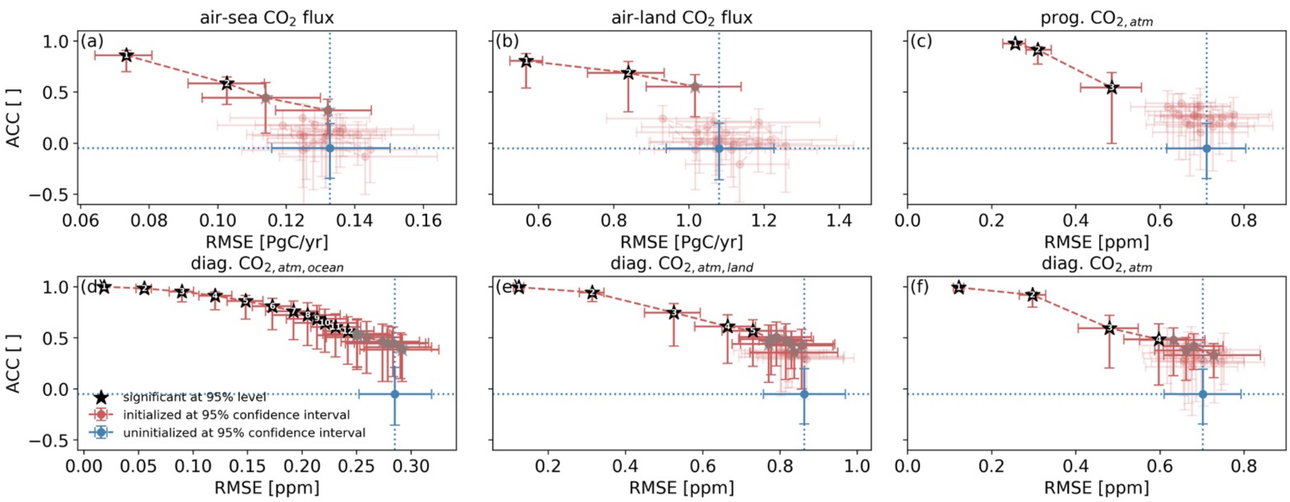


**Figure 3.2:** Comparison of the mean potential prediction skill of the initialized ensemble (red) versus random uninitialized ensembles (blue) in global annual surface quantities of the carbon cycle with the anomaly correlation coefficient (ACC) on the y axis and root-mean-square-error (RMSE) on the x axis for lead years

represented as dots: (a) air-sea CO2 flux, (b) air-land CO2 flux, (c) prognostic surface atmospheric CO2 , (d) diagnosed atmospheric CO2 based on oceanic carbon sink, (e) diagnosed atmospheric CO2 based on the global terrestrial carbon sink, and (f) diagnosed atmospheric CO2 based on the global oceanic and terrestrial carbon sink (see section 2.4). Error bars show 95% confidence intervals based on bootstrapping with replacement (N = 5,000). The last lead year with a bootstrapped p value (which represents that uninitialized ensembles beat initialized ensembles) lower than 5% marks the predictability horizon. Black stars with white integer denote significant lead years in ACC and RMSE, gray stars if only one metric is significant, and lead years nonsignificant in both metrics are blurred.

Moreover, MPG also used the 100-member MPI-ESM Grand Ensemble and compared global atmospheric CO2 variability and force trends in RCP2.6 containing emission reductions with RCP4.5 without CO2 emission reductions. They found that CO2 emissions caused a reduction in atmospheric CO2 5-year trends only by 42-22% depending on causation type. These probabilities are far from certain. Certainty in causation only arises after 10 years, which is much longer than the pentadal Global Stocktake periodicity (Figure 3.3). Initialized predictions may reduce this uncertainty stemming from internal variability. This work has been published on Environmental Research Letters (Spring et al., 2020).

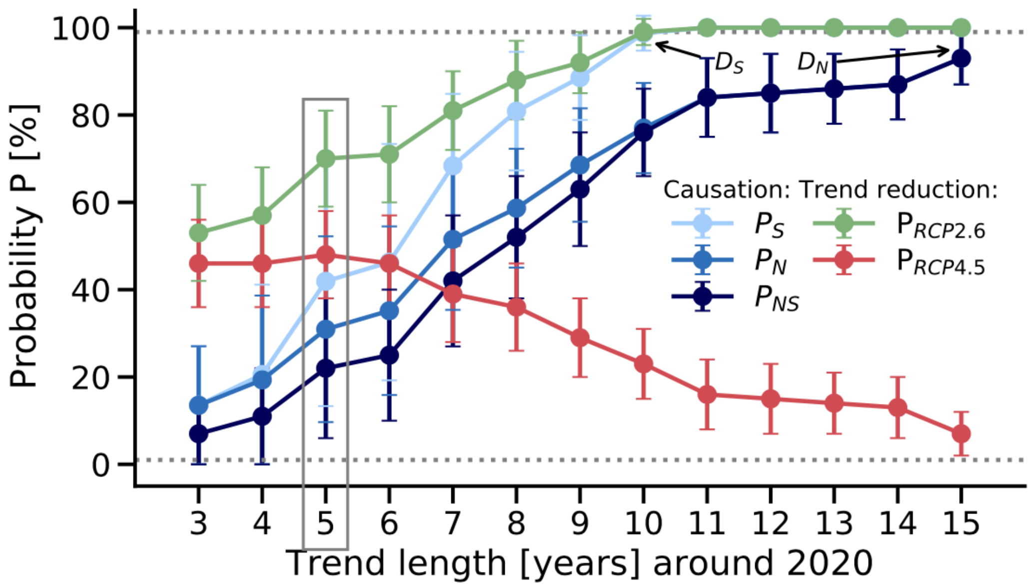


**Figure 3.3:** Probabilities of trend reduction in diagnostic atmospheric CO2 between periods of varying trend length before and after CO2 emission reductions start in 2020. PRCP2.6 (green) shows the probability of trend reduction in CO2 emission reductions scenario RCP2.6. PRCP4.5 (red) shows the probability of trend reduction in the currently most likely scenario for the near-term RCP4.5. P S (pale blue) show the probability that a change from RCP4.5 to RCP2.6 causes the respective trend reduction in a sufficient causation sense. PN (blue)show the probability that a change from RCP4.5 to RCP2.6 causes the respective trend reduction in

a necessary causation sense. PNS (dark blue) shows the probability that change from RCP4.5 to RCP2.6 causes the respective trend reduction in a sufficient and necessary causation sense. Error bars show the 1% and 99% confidence intervals based on bootstrapping with replacement. Dotted lines show 99% confidence interval for time of virtual certainty in trend reduction or causation (D{S,N}). Results for policy-relevant five-year trends are highlighted in the gray box.

## 3.3 EC-Earth3-CC

The perfect model prediction experiments performed with the EC-Earth3-CC model reveal that globally averaged ocean CO2 flux is predictable in average for more than 7 years but with very limited information after the 2$^{nd}$ forecast year (Figure 3.4-2$^{nd}$ column top). The globally averaged land CO2 fluxes is not predictable after the 2$^{nd}$ forecast year and only present limited predictability during the first 2 years of the forecast (Figure 3.4-3$^{rd}$ column top). The land CO2 fluxes variations are 10 times stronger than the ocean variations (Figure 5.1). Given the high level of noise in the land CO2 fluxes, the atmospheric CO2 concentration variations are only predictable up to two years with very limited precision.

At the regional scale, our analysis shows that land CO2 fluxes can be highly predictable at the forecast horizon 2 years (Figure 3.4-2$^{nd}$ column). In particular, we note high ACC values over Australia and the equatorial region of South America where the inter-annual variations of CO2 fluxes are high (cf. Figure 5.1 - top-left). Such high predictability at regional scale contrasts with the low predictability at global scale. This apparent paradox is due to an absence of covariability between the different land regions in EC-Earth3-CC (not shown). Over ocean, the CO2 fluxes can be predicted for more than 5 years in the Southern Ocean and the North Atlantic region (Figure 3.4-2$^{nd}$ column). Such long predictability horizon is consistent with the predictability of the physical properties in those regions (cf. Figure 3.4-1$^{st}$ column). Over land, only marginal areas show ACC significantly different from 0 after forecast year 2.

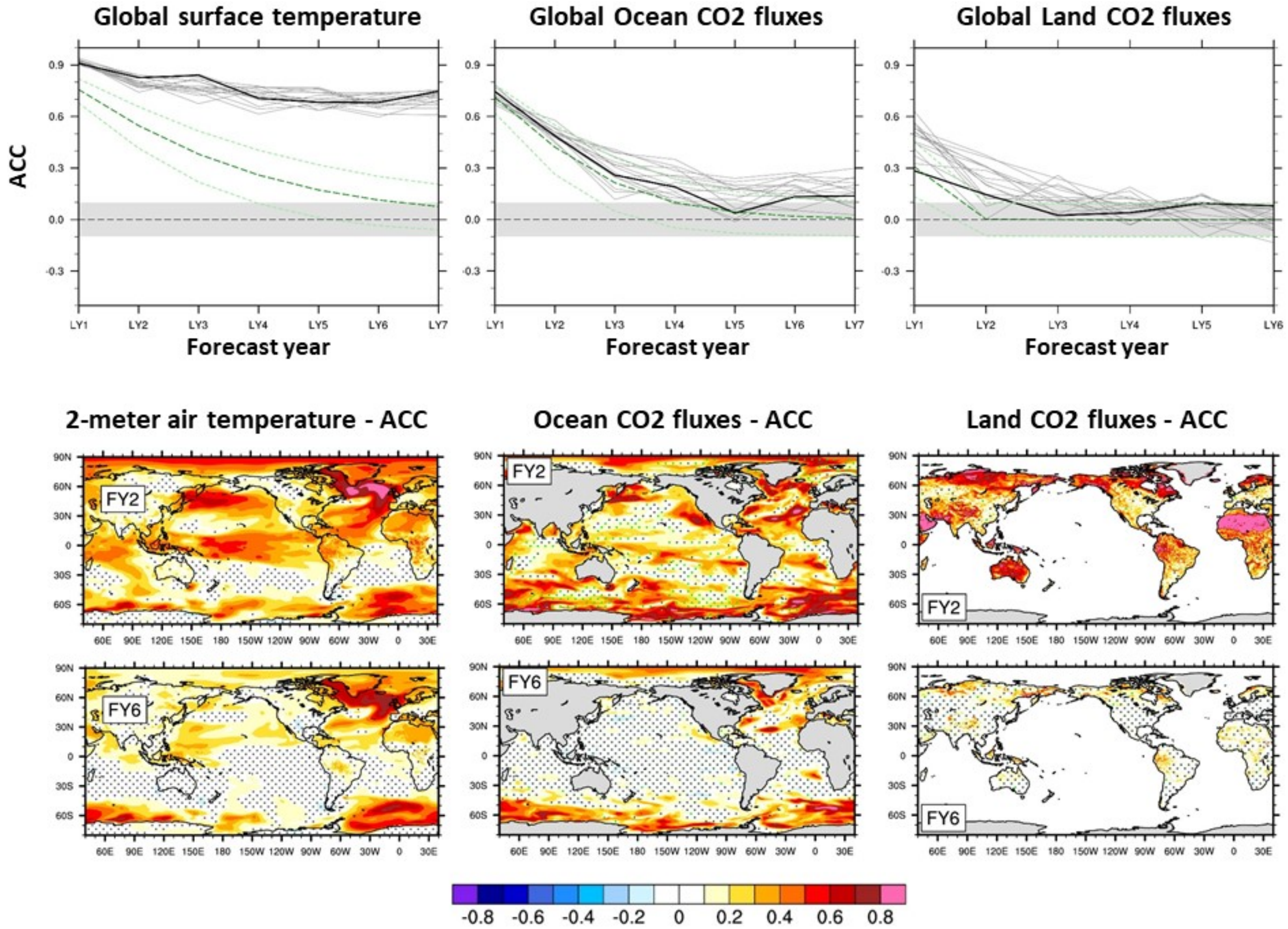


**Figure 3.4**: mean potential predictability of 2-meter air temperature (1st column), ocean surface CO2 fluxes (2nd column) and land surface CO2 fluxes (3rd column) estimated by the Anomaly Correlation Coefficient (ACC) from a perfect model approach with the EC-Earth3-CC piControl simulation. (1st row) ACC computed for the global averaged variables. The black line is the ACC computed considering the piControl trajectory as the target to predict. Each gray lines represent the ACC computed by considering a random prediction member as the target to predict (this informs on the uncertainty of our ACC estimate given the level of noise in the target to predict). The gray shading indicates the area in which the ACC is not significantly different from 0 (i.e. no more prediction skill) assessed with bootstrap resampling of the piControl simulation. The green lines indicate the ACC behavior of an hypothetical AR1 process fitted on the piControl behavior. (2nd row) ACC map computed for the forecast year 2. The stippling indicates where the ACC are not different from 0 according to bootstrap resampling. (3rd row) same as (2nd row) but for forecast year 6.

# 4 Potential predictability of ecosystem drivers

Although not initially planned, UBERN conducted a study in perfect model framework using the GFDL ESM2M model to assess the potential predictability of marine ecosystem drivers, such as temperature, pH, oxygen and net primary production. These parameters are also drivers of the ocean carbon cycle and thus are also relevant for the predictability of the ocean CO2 sink. UBERN shows that all four ecosystem drivers are potentially predictable on global scales and at the surface up to 3 years in advance. However, there are distinct regional differences in the potential predictability of these drivers (Figure 4.1). Maximum potential predictability (longer than 10 years) is found at the surface for temperature and oxygen in the Southern Ocean and for temperature, oxygen and pH in the North Atlantic. This is tied to ocean overturning structures with memory or inertia with enhanced predictability in Winter. In contrast, minimum predictability is simulated for net primary production in the Southern Ocean. Potential predictability increases with depth to more than 10 years below the thermocline. The paper has been published in Biogeosciences (Frölicher et al. 2020).

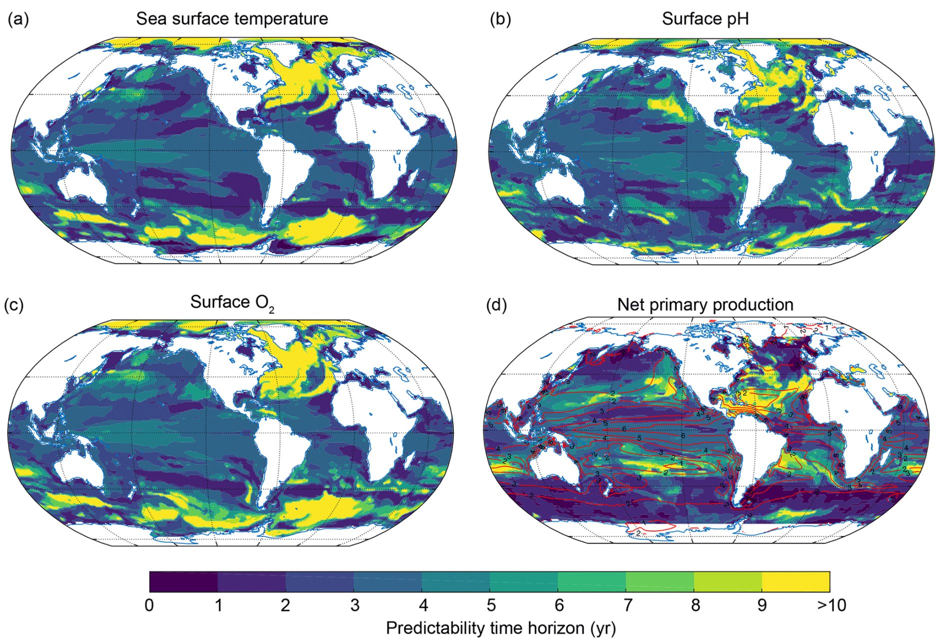


**Figure 4.1:** Predictability time horizon for (a) SST, (b) surface pH, (c) surface O2 and (d) NPP integrated over the top 100 m using PPP as a predictability measure. The red contour lines in panel (d) indicate the annual mean total nitrogen production in moles of nitrogen per kilogram per year averaged over the 300-year preindustrial control simulation to highlight regions with low and high NPP. In panel (d) regions north of 69◦ N and south of 69◦ S have been excluded since NPP is zero during wintertime there.

# 5 Potential predictability: processes, drivers and key regions

To understand the key regions controlling CO2 fluxes variability we analyzed the preindustrial piControl simulations from the three models. In Figure 5.1 the annual mean standard deviation for surface CO2 fluxes is represented for the land and ocean for the three models. The land fluxes have important inter-model differences with EC-Earth3-CC having the largest variability almost everywhere. Indeed, EC-Earth3-CC appears as an outlier in the distribution of the CMIP6 models considering the land CO2 flux variability (Figure 5.2 - left). Yet, important differences are also observed between the other two models, especially in Tropical South America and Africa. The variability patterns in the ocean seems to broadly agree across the three models with the high latitudes showing the largest standard deviations.

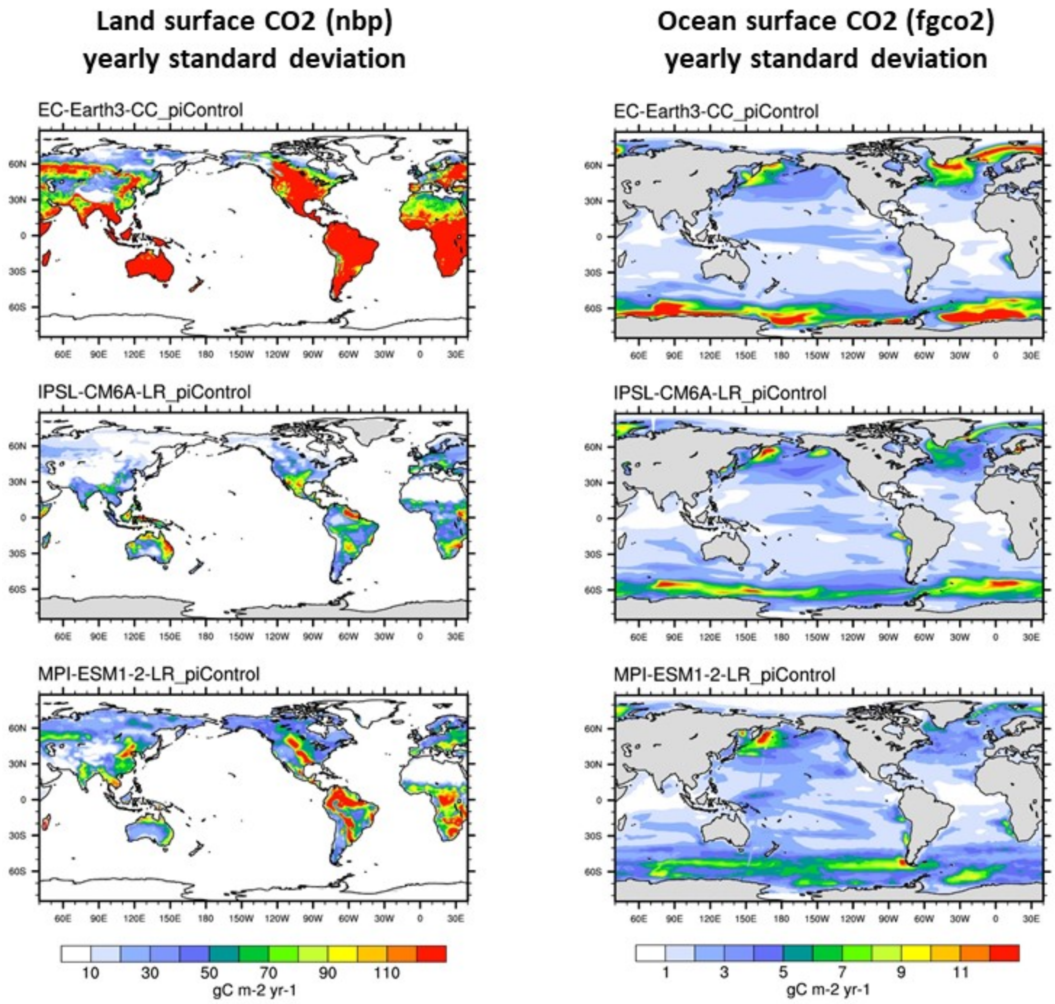

**Figure 5.1:** standard deviation of surface CO2 fluxes computed from annual mean of the piControl simulations of (top) EC-Earth3-CC, (middle) IPSL-CM6A-LR and (bottom) MPI-ESM1-2-LR over (left) land and (right) ocean. Note that the scales are different between land and ocean fluxes.

To assess the relative importance that the regional variability is playing in the global CO2 variations, we divide the globe in sub-regions (Figure 5.2). The land regions contributing the most to the global land CO2 variability are tropical America, Africa, Oceania and the extra-tropical region of the Northern Hemisphere, although the exact contributions of those regions vary among the three models. In the ocean, we find that the Southern Ocean is contributing for most of the global ocean CO2 variability followed by far by the tropical Pacific Ocean. However, looking at the CMIP6 model distribution, we acknowledge that our three models may be underestimating the importance of the tropical Pacific  Ocean.

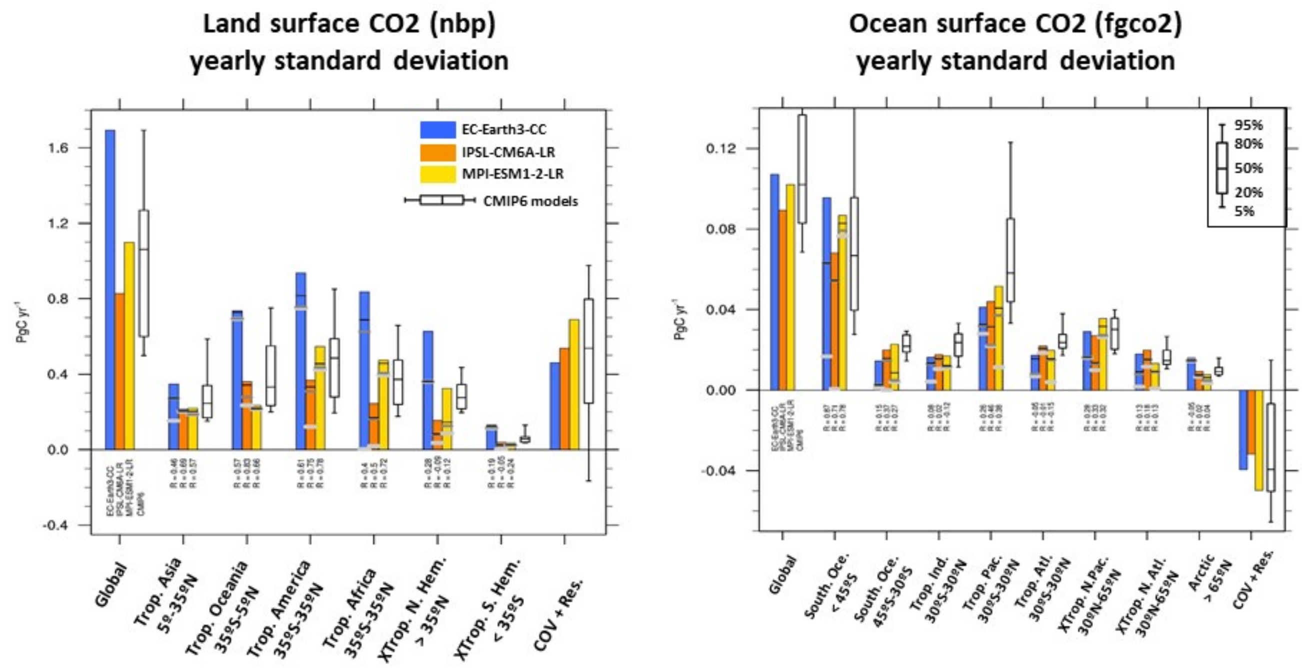


**Figure 5.2**: Standard deviation of annual mean surface CO2 fluxes integrated over different regions from the piControl simulations of EC-Earth3-CC (blue), IPSL-CM6A-LR (orange) and MPI-ESM1-2-LR (yellow). The box plots indicate the distribution of 21 CMIP6 piControl simulations (including the 3 models listed above). For each region the correlation (R) with the globally integrated CO2 fluxes is indicated at the bottom of the bar plot.

We compute correlation maps of surface temperature with the averaged CO2 fluxes over the regions contributing the most to the global variations. We find that, in the three models, the land CO2 variability over the tropics and the extra-tropical Northern Hemisphere are highly correlated with tropical SST variability, especially in the tropical Pacific (Figure 5.3). This suggests that the tropical Pacific variability is driving most of the land CO2 fluxes variability.

In the ocean, we see that the tropical Pacific CO2 variations are linked to an ENSO signal in EC-Earth3-CC and IPSL-CM6A-LR but not in MPI-ESM1-2-LR (Figure 5.4). Regarding the Southern Ocean, the SST patterns are also different among models. Especially, in the MPI-ESM1-2-LR the ocean CO2 fluxes variations are linked to SST anomalies in the tropical Pacific but not in EC-Earth3-CC and IPSL-CM6A-LR. The SST patterns of those  latter two models are more similar. Yet, we found that the temporal characteristics of the Southern Ocean CO2 variability are different between those two models. An oscillation with a period of 15-20 years is present EC-Earth3-CC but not in IPSL-CM6A-LR nor in MPI-ESM1-2-LR. Further analyses are ongoing to understand those model differences.

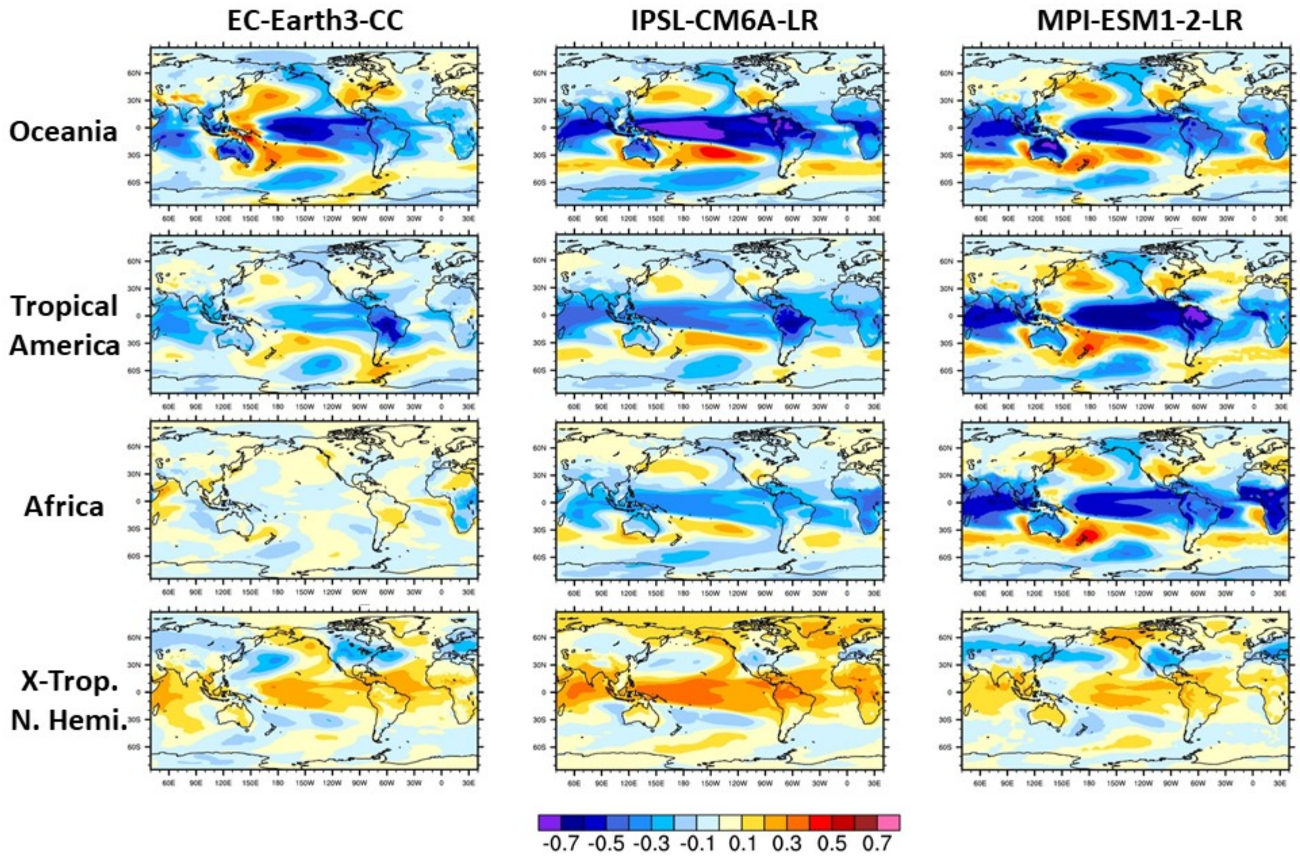


**Figure 5.3**: Spatial correlation of the 2-meter air temperature with the time series of the land surface CO2 fluxes integrated over (top) Oceania, (2nd row) Tropical America, (3rd row) Africa and (bottom) extra-tropical Northern Hemisphere land for (left) EC-Earth3-CC, (middle) IPSL-CM6A-LR and (right) MPI-ESM1-2-LR.

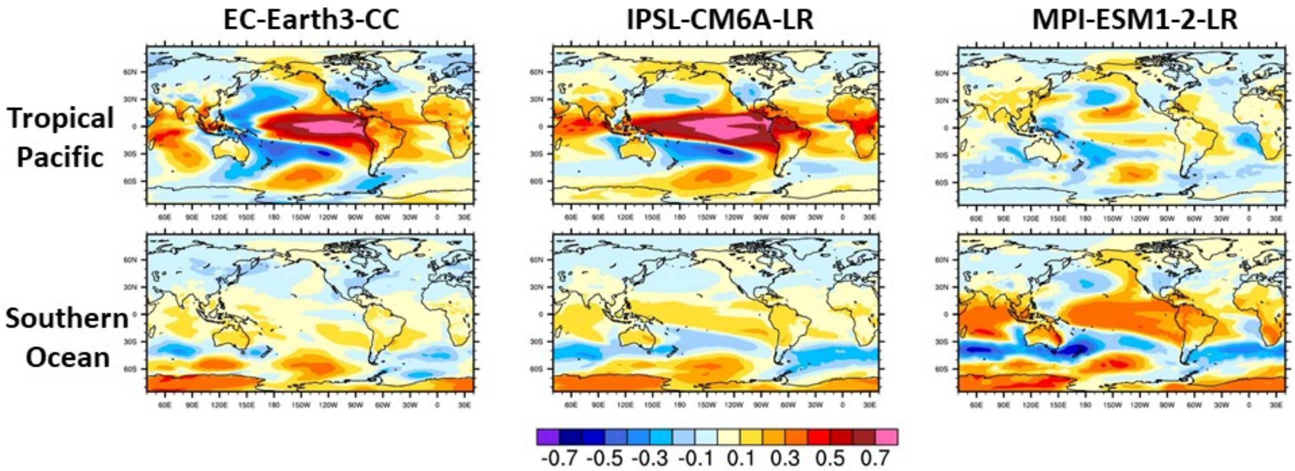


**Figure 5.4**: same as Figure 5.3 but for the ocean surface CO2 fluxes integrated over (top) the tropical Pacific and (bottom) the Southern Ocean South of 45ºS.

MPG plans a publication comparing the 4C models (MPI-ESM, EC-Earth, IPSL-ESM and GFDL-ESM, see Figure 5.5) and other ESMs (such as NorESM, CanESM, MIROC-ESM) in a multi-model perfect-model carbon cycle predictability study. Such a study highlights the similar predictability horizons of the global carbon cycles in all models, but shows the spatial heterogeneity of CO2 flux predictability.

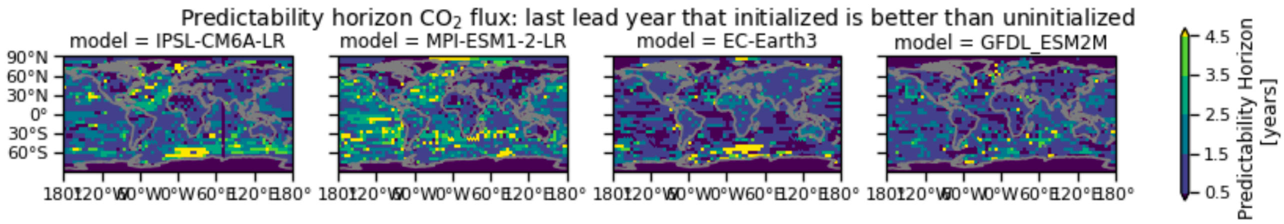


**Figure 5.5:** Predictability horizon of air-sea and air-Land co2 flux defined as latest lead year where initialised skill is better than uninitialised skill for four ESMs.

Currently state-of-the-art carbon cycle prediction models do not initialize carbon cycle variables, but only physical climate variables. To assess the importance of reconstruction and initial conditions on carbon cycle predictability, MPG conducted perfect-model reconstruction and predictability experiments. We find that reconstructing the carbon cycle shows only small improvements for its predictability (Figure 5.6). A bias reconstruction mostly brings similar improvements. Reconstructing the physical climate variables is sufficient to reconstruct CO2 flux variations, and therefore an appropriate choice given the sparse and short observational record. These results are currently under discussion in ESDD (Spring et al, 2021).

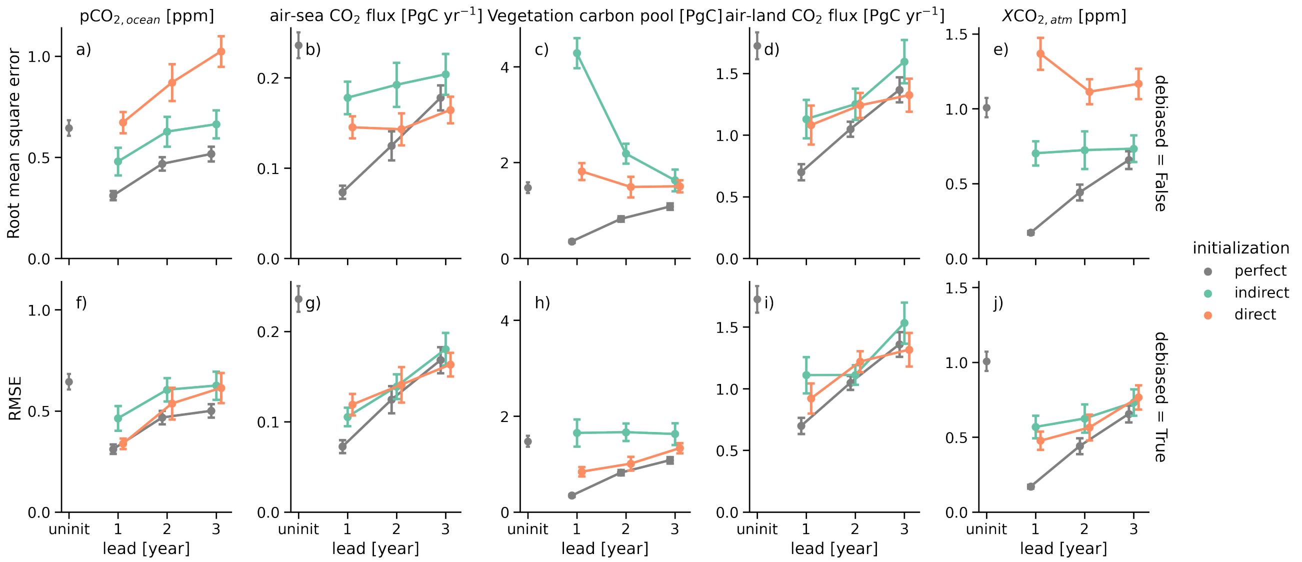


**Figure 5.6:** Predictive skill measured by root-mean-square-error (RMSE) between the initialized ensemble mean and the target as a function of lead year for different initialization setups: perfect indicating no reconstruction and hence perfect initial conditions to predict the target (gray), indirect (green) and direct (orange). Columns show global variables: for the ocean carbon cycle (a) oceanic surface pCO2 , (b) air-sea CO2 flux; for the land carbon cycle (c) total land carbon pools, (d) air-land CO2 flux and in the atmosphere (e) atmospheric CO2 mixing ratio. (f-j) show RMSE-based predictive skill as (a-e) after mean bias reduction. Initialized ensembles are resampled with replacement (N=500) along the initialization dimension to account for initialization sampling uncertainty (see Spring and Ilyina, 2020), where errorbars show the resampled initialization skill uncertainty (±1σ). Uninitialized ensembles, shown at lead 0, are resampled from the target control simulation and show the reference skill without initialization.

In order to gain understanding on the importance of the tropical Pacific for the global air-sea CO2 flux, the consortium has decided to analyze coordinated experiments. Given the importance of the tropical Pacific for both oceanic and land co2 flux (Fig. 5.3 and 5.4), it has been decided to exploit the DCPP-C1.10 so-called" Pacific Pacemaker experiment" (Boer et al 2016), for which the Pacific Ocean SST is constrained towards the observed SST anomalies over the historical period. The objective of this protocol is to quantify the constrain that the tropical Pacific SST exerts on the air-sea CO2 fluxes. Fig 5.7 shows preliminary results from existing simulations with the IPSL-CM6A-LR climate model. Global mean SST is strongly constrained by the tropical Pacific nudging (top panel) but on this figure, in this model, the global mean CO2 does not seem to be. Ongoing analysis will investigate more thoroughly the impact of the SST nudging on specific basins with the objective of performing the simulations with the three ESMs. Furthermore, in case other modeling groups external to the consortium decide to perform these experiments which are part of the DCPP protocol, we will consider including their model in the common analysis so as to increase robustness of the results.

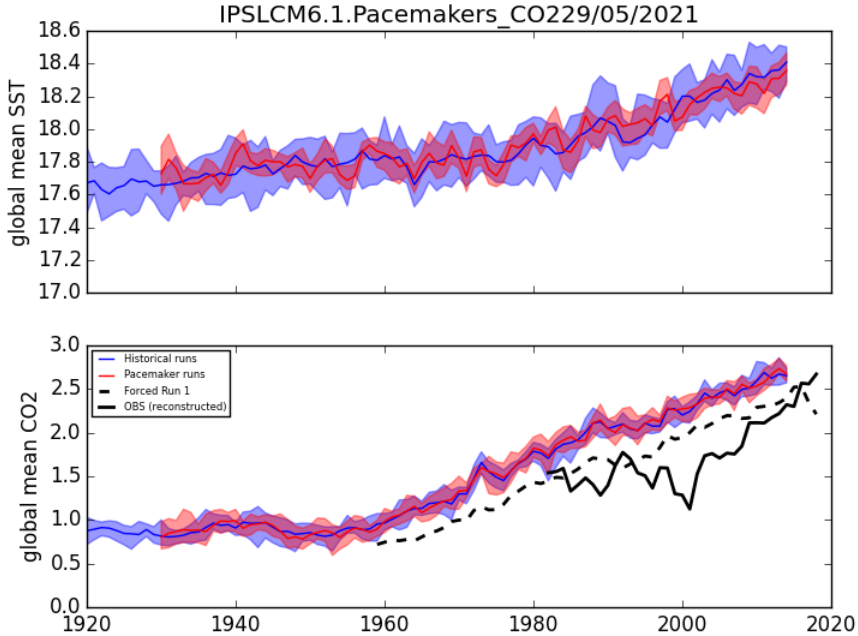


**Figure 5.7:** global mean temperature (top, °C) and total CO2 flux into the ocean (bottom, PgC) in the 10-mb ensemble of historical (blue) and Pacific Pacemaker (red) experiments performed with IPSL-CM6A-LR. The continuous line shows the ensemble mean and the shading the minimum and maximum values reached for each year in the 10-mb ensemble. The black line shows the data-based estimate, resulting from the average of the MPI-SOMFFN (Landschutzer et al. 2016), Jena-MLS (Roedenbeck et al. 2015) and CMEMS (Denvil-Sommer et al. 2019) products. The black-dash line shows the ocean forced simulation with NEMO-PISCES used for the Global Carbon Budget 2019 (Friedlingstein et al. 2019).

# 6 Conclusions

We quantified potential predictability of global CO2 fluxes for 3 Earth System Models using perfect model predictions that take as a reference a preindustrial control simulation. We found an overall agreement across models with global ocean CO2 fluxes having a longer predictability (7-12 years) than global land CO2 fluxes (2-5 years). However, the latter, because of its larger variability, limits the predictability of atmospheric CO2. From an inter-model comparison of land and ocean CO2 fluxes variability we have found important differences across models on land fluxes while overall the three models seem to broadly agree over the ocean where high latitudes have the largest variability. However, when correlating local surface temperature with regional averages of CO2 fluxes we found the tropical Pacific variability to significantly correlate with several region’s land CO2 flux variability. On the other hand, similar correlations for the ocean revealed important differences across the three ESMs on the strength of the correlation between this region and the regional oceanic CO2 fluxes. Given the importance of the tropical Pacific for both oceanic and land CO2 fluxes, we decided to analyze results from the DCPP-C1.10 so-called ”Pacific Pacemaker experiment”, for which the Pacific Ocean SST is constrained towards the observed anomalies over the historical period. While global mean SST is strongly constrained by the tropical Pacific, global mean CO2 flux does not seem to be. However, this conclusion is based on only one ESM so far and the consortium is currently running more pacemaker experiments to investigate also the impact of different regions besides the tropical Pacific.

Importantly, other studies were carried out using the perfect model framework. One ESM was used to investigate the potential predictability of marine ecosystem drivers, finding that all four drivers considered (temp., pH, O2 and net primary production) are potentially predictable at the surface on global scales up to 3 years in advance with however important regional differences. In another study one ESM was used to investigate the impact direct initialization of carbon cycle variables have on the predictability of atmospheric CO2, finding only a marginal improvement. These results confirm that the assimilation of physical climate variables is sufficient to reconstruct CO2 flux variations, and therefore an appropriate choice given the sparse and short observational record of carbon cycle variables.

# 7 Publications

Spring, A., Ilyina, T. (2020). Predictability horizons in the global carbon cycle inferred from a perfect-model framework. Geophysical Research Letters, 47, https://doi.org/10.1029/2019GL0853111

Spring, A., Ilyina, T. and Marotzke, (2020). Inherent uncertainty disguises attribution of reduced atmospheric CO2 growth to CO2 emission reductions for up to a decade. Environmental Research Letters, 15, 114058, https://doi.org/10.1088/1748-9326/abc443

Spring, A., Dunkl, I., Li, H., Brovkin, V., and Ilyina, T.: Trivial improvements of predictive skill due to direct reconstruction of global carbon cycle, Earth Syst. Dynam. Discuss. [preprint], https://doi.org/10.5194/esd-2021-4, in review, 2021.

Frölicher, T. L., Ramseyer, L., Raible, C. C., Rodgers, K. B., and Dunne, J. (2020). Potential predictability of marine ecosystem drivers. Biogeosciences, 17, 2061–2083, https://doi.org/10.5194/bg-17-2061-2020, 2020

Ruprich-Robert, Y., Bernardello, R., Tourigny, E., Ortega, P., Sicardi, V. And Lapin, V. Conditional predictability of CO2 fluxes on the initial climatic state in an Earth System Model. *In prep.*

Menary, M., Mosneron, C., Mignot, J., Bopp, M. Mechanisms of interannual to multidecadal variability of CO2 flux in the ocean. *In prep.*

# 8 References


Boer, G.J. Decadal potential predictability of twenty-first century climate. Clim Dyn 36, 1119–1133 (2011). https://doi.org/10.1007/s00382-010-0747-9

Boer, G. J., Smith, D. M., Cassou, C., Doblas-Reyes, F., Danabasoglu, G., Kirtman, B., Kushnir, Y., Kimoto, M., Meehl, G. A., Msadek, R., Mueller, W. A., Taylor, K. E., Zwiers, F., Rixen, M., Ruprich-Robert, Y., and Eade, R.: The Decadal Climate Prediction Project (DCPP) contribution to CMIP6, Geosci. Model Dev., 9, 3751–3777, https://doi.org/10.5194/gmd-9-3751-2016, 2016.

Denvil-Sommer, A., Gehlen, M., Vrac, M., and Mejia, C.: LSCE-FFNN-v1: a two-step neural network model for the reconstruction of surface ocean $pCO_2$ over the global ocean, Geosci. Model Dev., 12, 2091–2105, https://doi.org/10.5194/gmd-12-2091-2019, 2019.

Friedlingstein, P., Jones, M., O'sullivan, M., Andrew, R., Hauck, J., Peters, G., et al. (2019). Global carbon budget 2019. Earth System Science Data, 11 (4), 1783-1838.

Landschützer, P., Gruber, N., Haumann, F. A., Rodenbeck, C., Bakker, D. C., Van Heuven, S., et al. (2015). The reinvigoration of the southern ocean carbon sink. *Science*, 349 (6253), 1221-1224.

Rödenbeck, C., Bakker, D. C. E., Gruber, N., Iida, Y., Jacobson, A. R., Jones, S., Landschützer, P., Metzl, N., Nakaoka, S., Olsen, A., Park, G.-H., Peylin, P., Rodgers, K. B., Sasse, T. P., Schuster, U., Shutler, J. D., Valsala, V., Wanninkhof, R., and Zeng, J.: Data-based estimates of the ocean carbon sink variability – first results of the Surface Ocean $pCO_2$ Mapping intercomparison (SOCOM), Biogeosciences, 12, 7251–7278, https://doi.org/10.5194/bg-12-7251-2015, 2015.